

Chemical Science

Accepted Manuscript

This article can be cited before page numbers have been issued, to do this please use: B. Chartier, L. MARCHETTI, L. M. A. Ali, D. AKL, G. Micouin, A. Banyasz, S. MEME, D. Boturyn, S. Erbek, V. Martel-Frchet, A. Grichine, O. Maury, M. Gary-Bobo, C. S. Bonnet and O. Sénèque, *Chem. Sci.*, 2026, DOI: 10.1039/D5SC06902E.



This is an Accepted Manuscript, which has been through the Royal Society of Chemistry peer review process and has been accepted for publication.

Accepted Manuscripts are published online shortly after acceptance, before technical editing, formatting and proof reading. Using this free service, authors can make their results available to the community, in citable form, before we publish the edited article. We will replace this Accepted Manuscript with the edited and formatted Advance Article as soon as it is available.

You can find more information about Accepted Manuscripts in the [Information for Authors](#).

Please note that technical editing may introduce minor changes to the text and/or graphics, which may alter content. The journal's standard [Terms & Conditions](#) and the [Ethical guidelines](#) still apply. In no event shall the Royal Society of Chemistry be held responsible for any errors or omissions in this Accepted Manuscript or any consequences arising from the use of any information it contains.

ARTICLE

Lanthanide Complexes with Acetophenone-based Push-Pull Antenna as Efficient MRI and Two-Photon Microscopy Imaging Probes

Baptiste Chartier,^{a,b} Luke Marchetti,^c Lamiaa M. A. Ali,^d Dina Akl,^e Guillaume Micouin,^e Akos Banyasz,^e Sandra Môme,^c Didier Boturyn,^b Sule Erbek,^{f,g} Véronique Martel-Fachet,^{f,g} Alexei Grichine,^f Olivier Maury,^e Magali Gary-Bobo,^{*d} Célia S. Bonnet,^{*c} Olivier Sénèque^{*a}

Received 00th January 20xx,
Accepted 00th January 20xx

DOI: 10.1039/x0xx00000x

Lanthanide(III) (Ln³⁺) complexes possess unique magnetic and optical properties that make them ideal candidates for the development of multimodal MRI and optical probes. However, the requirements for developing effective MRI and optical probes are difficult to meet within a single ligand. Here, we propose the use of a DOTA-type ligand equipped with a π -extended acetophenone moiety that (i) serves as a coordinating moiety to form stable Ln³⁺ complexes, (ii) acts as a 2P-excitabile push-pull antenna to sensitize Eu³⁺ luminescence, and (iii) displays a carboxylate handle offering high water solubility and enabling conjugation to biomolecules for targeting purposes. We show that the Ln³⁺ complexes obtained are kinetically inert and thermodynamically stable. The Gd³⁺ complex exhibits positive *in vivo* characteristics with good contrast in all organs and rapid renal clearance, while the corresponding Eu³⁺ complex has excellent one-photon and two-photon (2P) absorption properties enabling high-quality *in vivo* 2P microscopy imaging of zebrafish embryos or *in vitro* imaging of living cells when conjugated to a cell-penetrating peptide.

Introduction

Over the past number of decades, lanthanide complexes have been implemented to great success in various modalities in the field of biological imaging. Luminescent lanthanide complexes possess many advantageous properties for optical techniques, such as narrow emission bands at fixed wavelengths that are specific to each lanthanide, long luminescence lifetimes, and resistance to photobleaching.^{1,2} Indeed, there are numerous examples of luminescent lanthanide complexes, such as those containing Eu³⁺, Tb³⁺ or Yb³⁺, being exploited for not only cellular imaging^{3–8} but also for detection of various analytes.^{3,9–12} Magnetic resonance imaging (MRI) is an imaging technique, endowed with unlimited tissue depth penetration and excellent spatiotemporal resolution. The exploitation of Gd³⁺-based

contrast agents (CA) in MRI has allowed for improved diagnostic accuracy,¹³ as well as having the option to incorporate targeting moieties into the CA¹⁴ or render it “responsive”,^{12,15,16} enabling the selective detection of various biological relevant species – including but not limited to cations,^{17–19} extracellular proteins,²⁰ and neurotransmitters.²¹

These two imaging modalities are not without their own drawbacks, however. While luminescent techniques display high sensitivity, they suffer from low macroscopic resolution and often require the integration of a cell-internalization vector, such as a peptide, to penetrate into living cells. Meanwhile, MRI has high macroscopic resolution but low sensitivity, requiring high concentrations of CAs to be detected. In recent years, the development of imaging probes active in both modalities has seen increased traction.^{22–31} By incorporating complementary imaging modalities within a single molecular design, one could achieve non-invasive, real-time monitoring with high sensitivity and resolution, effectively overcoming the limitations of the individual imaging modalities.^{24,27,28} This would also have the benefit of complementary imaging at different scales, enabling monitoring of cellular processes and the anatomical context in real time.

Lanthanide complexes are particularly well-situated for these applications because of their different optical and magnetic properties across the series while still maintaining similar coordination properties and chemical reactivities. However, the development of pairs of lanthanide complexes relying on the same ligand, but displaying both MRI and luminescent activities are not without their own set of hurdles, either. MRI CAs require at least one inner-sphere coordinated

^a Univ. Grenoble Alpes, CNRS, CEA, IRIG, LCBM (UMR 5249), F-38000 Grenoble, France. E-mail: olivier.seneque@univ-grenoble-alpes.fr

^b Univ. Grenoble Alpes, CNRS, DCM (UMR 5250), F-38000 Grenoble, France.

^c Centre de Biophysique Moléculaire, CNRS (UPR 4301), Université d'Orléans, F-45041 Orléans, France. E-mail: celia.bonnet@cnrs.fr

^d IBMM, Univ Montpellier, CNRS, ENSCM, F-34000 Montpellier, France. E-mail: magali.garybobo@umontpellier.fr

^e Univ Lyon, ENS de Lyon, CNRS UMR 5182, Laboratoire de Chimie, Lyon F-69342, France.

^f Univ. Grenoble Alpes, INSERM U1209, CNRS UMR 5309, Institute for Advanced Biosciences, F-38000 Grenoble, France.

^g EPHE, PSL Research University, 4-14 rue Ferrus, 75014 Paris, France.

Supplementary Information available: Procedures for the synthesis of new compounds, 1P and 2P spectroscopy (absorption, luminescence), relaxometry, stability and inertness assays by luminescence; protocols for MRI experiments, toxicity assays and 2P microscopy imaging of zebrafish embryos, cell culture, toxicity assays and 2P microscopy imaging. See DOI: 10.1039/x0xx00000x



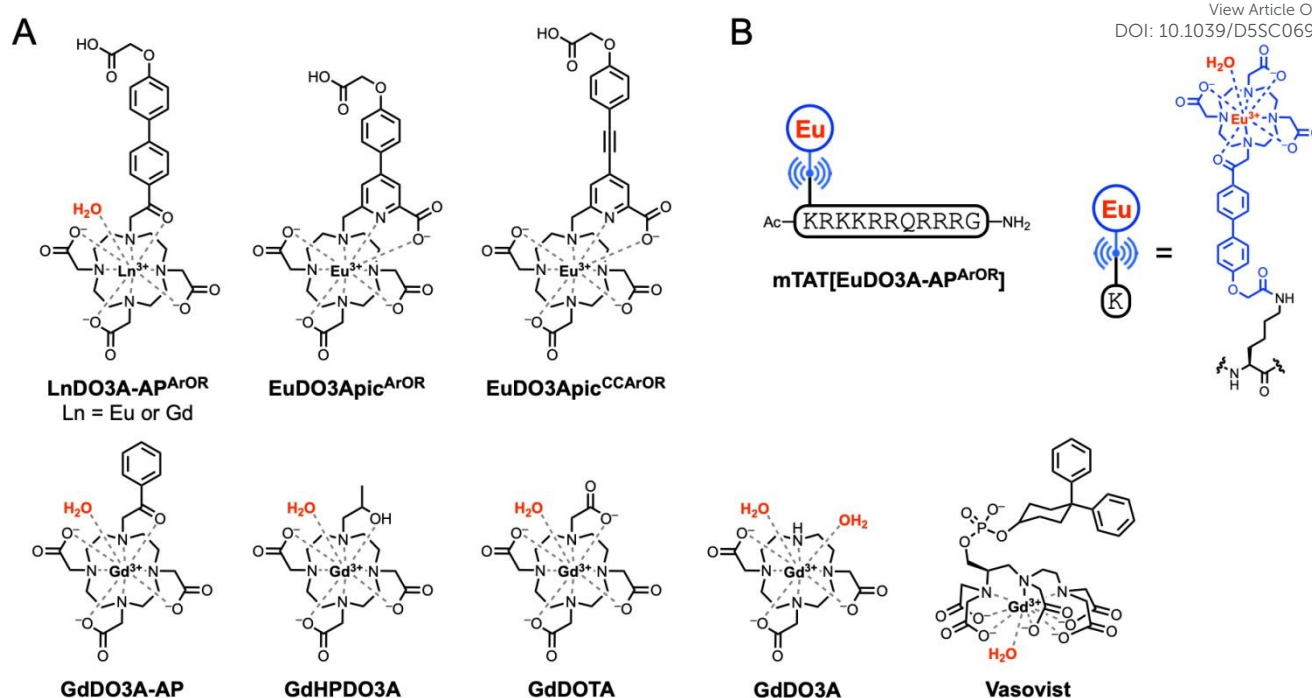


Fig. 1 Structure of (A) complexes LnDO3A-APArOR (Ln = Eu or Gd), EuDO3ApicArOR, EuDO3ApicCCArOR, GdDO3A-AP, GdHPDO3A, GdDOTA, GdDO3A and Vasovist, all discussed in the text and (B) conjugate mTAT[EuDO3A-APArOR].

water molecule to the Gd³⁺-center for efficient reduction of the T₁ relaxation time of water protons. This can be seen as incompatible with luminescent complexes which usually display a saturated coordination sphere, as directly coordinated water molecules quench lanthanide luminescence due to non-radiative deactivation.

Moreover, luminescent lanthanide complexes suffer from low molar absorption coefficients with values of about 1 to 5 M⁻¹ cm⁻¹, due to the Laporte rule that forbids the f-f transition. Nevertheless, this can be bypassed by the well-documented 'antenna effect', whereby a chromophore is implemented close to the lanthanide.^{2,12,32} This chromophore should efficiently absorb light, typically in the ultraviolet (UV) range, followed by subsequent energy transfer to the lanthanide, thus allowing for the sensitization of the lanthanide and resulting luminescence emission. It is important to note, that the use of UV light to excite the antenna is problematic, as UV light has not only been proven to be cytotoxic, but can be absorbed and scattered by biological tissues. An alternative to this excitation pathway is the use of a two-photon (2P) absorption process that allows for the simultaneous absorption of two photons, with half the energy required for a normal excitation with one photon.^{33–36} This method allows for a bathochromic shift of the excitation wavelength, moving from the UV to the red or near infrared, which is known to be less toxic and is scattered less by biological tissues. Unlike MRI, one of the main drawbacks of luminescence is its low tissue penetration. 2P excitation in the NIR allows deeper tissue penetration, thus compensating for the limitation of fluorescence imaging.^{37,38}

We have recently developed 2P excitable Ln³⁺ probes that were used successfully for 2P microscopy of live cells.^{39–43} These

probes are based on a DO3Apic ligand that saturates the Ln³⁺ coordination sphere, precluding their use as MRI CA. With the aim to design an octadentate Ln³⁺ chelator that leaves a single water molecule in the coordination sphere of the Ln³⁺ and features a 2P absorbing antenna, we identified in the literature DO3A-AP. This ligand was first reported to bind Eu³⁺ and sensitize its luminescence through the acetophenone antenna.⁴⁴ EuDO3A-AP is mono-hydrated and shows a Eu³⁺ luminescence quantum yield of 0.058 upon excitation in the acetophenone absorption band at 265 nm. The absorption could be red-shifted by introducing electron-rich methoxy⁴⁴ or triazole⁴⁵ groups in the *para*- position of the acetophenone or by substituting the phenyl-ketone by other aryl-ketones (aryl = naphthyl, carbazolyl or phenantrenyl).⁴⁶ The relaxometric properties of GdDO3A-AP and related derivatives with hydroxy substituents were recently described.^{47,48} However, the *in vivo* MRI (with Gd³⁺ as Ln³⁺) or *in vitro/in vivo* microscopy imaging (with Eu³⁺) capacities of the LnDO3A-AP system were never explored.

Based on this, we wanted to push the advantage and propose for the first time a monohydrated Ln³⁺ complex for both high resolution 2P microscopy, with Eu³⁺ as the Ln³⁺, and MRI, with Gd³⁺. We present here DO3A-APArOR (Fig. 1), a ligand derived from DO3A-AP bearing an antenna with strong push-pull capabilities providing 2P absorption properties and a reactive handle for the facile incorporation of a cell-penetrating peptide. The coordination sphere remains unsaturated, allowing for one water molecule in the inner-sphere, granting the opportunity for its use as an MRI contrast agent. The photophysical properties of the Eu³⁺ complex were investigated, alongside its two photon excitation properties,



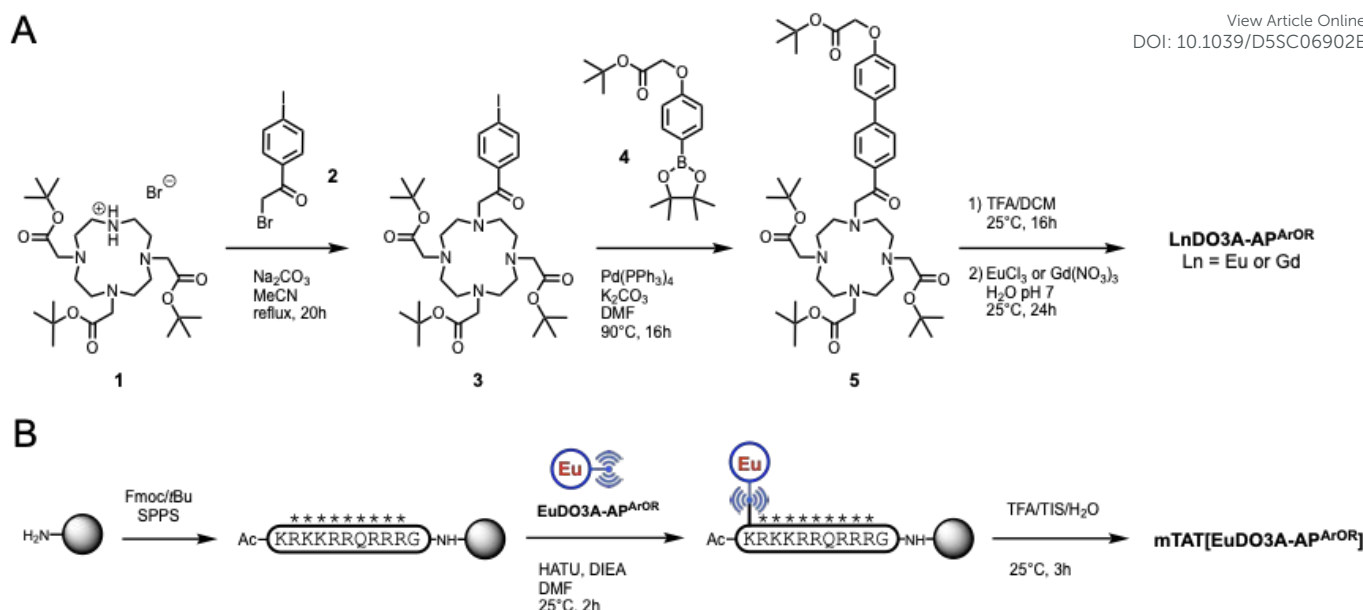


Fig. 2 Synthetic pathway for (A) **EuDO3A-AP^{ArOR}** and **GdDO3A-AP^{ArOR}** and (B) **mTAT[EuDO3A-AP^{ArOR}]**. In B, * denote standard side chains protecting groups.

and compared to the previously described non-hydrated picolinate analogues **EuDO3Apic^{ArOR}** and **EuDO3Apic^{CCArOR}**^{39,43}. Despite its coordinated water molecule, **EuDO3A-AP^{ArOR}** shows good luminescence properties. The relaxometric properties of the **Gd³⁺** complex were characterized by variable temperature ¹⁷O NMR experiments and nuclear magnetic relaxation dispersion. The complex also displays very high kinetic inertness. These positive features allow for the *in vivo* use of the **Gd³⁺** complex as an efficient MRI contrast agent, and the **Eu³⁺** complex as a luminescent probe for 2P microscopy in zebrafish. A cell-penetrating peptide, mTAT, was conjugated to the antenna which allowed for internalization of the complex to the cytosol of live HeLa cells, visualized by 2P microscopy. Therefore, this versatile design based on a Ln³⁺ complex allows *in vivo* MRI in mice and 2P microscopy on zebrafish, as well as high quality cell imaging by 2P microscopy.

Results and discussion

Synthesis of the ligand and its lanthanide complexes

The synthetic pathway for the preparation of the acetophenone-based Ln³⁺ complexes is depicted in Fig. 2A. The synthesis starts with the alkylation of **DO3A(tBu)₃** **1**⁴⁹ with 2-bromo-1-(4-iodophenyl)ethan-1-one **2** in MeCN to give compound **3** in 94 % yield. A Miyaura-Suzuki coupling between **3** and boronic ester **4**⁴³ in DMF with polymer-bound Pd(PPh₃)₄ as a catalyst affords the tBu-protected ligand **5** in 56 % yield. After acidolysis of the tBu esters in a TFA/DCM mixture, metalation with Eu³⁺ or Gd³⁺ salt in water (pH 7) followed by HPLC purification and freeze-drying gives complexes **LnDO3A-AP^{ArOR}** in 80-90 % yield. Note that these compounds are sensitive to basic conditions, which can cause N-dealkylation of the acetophenone arm. The detailed synthetic procedures and NMR, HPLC and mass spectrometry characterizations of these compounds are given in the ESI.

Photophysical properties

The photophysical properties of the **EuDO3A-AP^{ArOR}** complex were investigated in phosphate-buffered saline (PBS, pH 7.4). The absorption spectrum of **EuDO3A-AP^{ArOR}** shows a broad structureless band in the UV with a maximum at 342 nm (λ_{max}) and extending up to 403 nm ($\lambda_{\text{cut-off}}$), which is assigned to an intra-ligand charge transfer transition (ILCT) within the antenna from the anisole donor to the coordinated carbonyl acceptor moieties (Fig. 3). This absorption is red-shifted by *ca.* 35 nm and 10 nm (Fig. S8) compared to the picolinate analogues **EuDO3Apic^{ArOR}** and **EuDO3Apic^{CCArOR}** (Fig. 1) with alkoxy-phenyl-picolinate and alkoxy-phenyl-ethynyl-picolinate antennas, respectively.^{39,43} The molar absorption coefficient of **EuDO3A-AP^{ArOR}** was determined to be 20000 M⁻¹ cm⁻¹ at λ_{max} (Fig. S9) similar to **EuDO3Apic^{ArOR}** (21000 M⁻¹ cm⁻¹)⁴³ and **EuDO3Apic^{CCArOR}** (21000 M⁻¹ cm⁻¹).³⁹ Upon excitation into the ILCT band at 340 nm, the Eu³⁺ emission is observed with ⁵D₀ → ⁷F_J transitions (J = 0, 1, 2, 3 and 4) at 580, 595, 615, 650 and 700 nm, respectively. The excitation spectrum (λ_{em} = 615 nm) matches well with the absorption spectrum, confirming that the alkoxy-phenyl-acetophenone antenna sensitizes Eu³⁺ luminescence. The Eu³⁺ luminescence decay could be perfectly fitted with a mono-exponential giving a lifetime value of 0.53 (2) ms (Fig. S10), which is about half that of the picolinate analogues **EuDO3Apic^{ArOR}** and **EuDO3Apic^{CCArOR}** (1.1 ms) with a saturated Eu³⁺ coordination sphere (hydration number *q* = 0).^{39,43} The lifetime remains unchanged upon degassing the solution. In PBS prepared with D₂O, the Eu³⁺ decay lifetime was 1.49 ms. According to Parker's equation, a hydration number *q* of 1.2 (2) was calculated from the lifetimes in H₂O and D₂O,⁵⁰ indicating that a single water molecule stands in the coordination sphere of Eu³⁺. This is in agreement with the literature on Ln³⁺ complexes of **DO3A-AP** ligands.⁴⁴⁻⁴⁸ The Eu³⁺ emission quantum yield, Φ_{Eu} , is 0.075 (Fig. S11), again almost



half that of the picolinate analogues (0.14 and 0.17 for EuDO3Apic^{ArOR} and EuDO3Apic^{CCArOR}, respectively).^{39,43} The energy of the alkoxy-phenyl-acetophenone antenna triplet state, T_1 , is 21100 cm⁻¹ (determined from the onset of the phosphorescence emission of GdDO3A-AP^{ArOR} at 77 K), which is 2000 cm⁻¹ below that of the picolinate analogue (Figure S12).⁴³ However, the antenna T_1 state remains high enough to prevent efficient back energy transfer from the Eu³⁺ 5D_0 excited state. In the end, EuDO3A-AP^{ArOR} is half as bright as its picolinate analogue because of the presence of one Eu³⁺-bound water molecule.

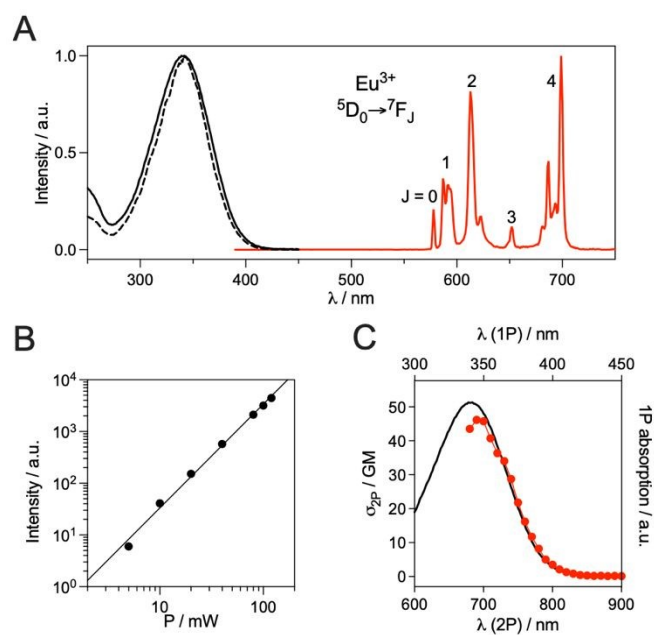


Fig. 3 (A) 1P spectroscopy: Normalized absorption (black solid lines), excitation (black dashed lines; λ_{em} = 615 nm) and emission (red solid lines; λ_{ex} = 340 nm) spectra of EuDO3A-AP^{ArOR} in PBS, pH 7.4. (B and C) 2P spectroscopy: (B) Quadratic power dependence of the Eu³⁺ emission (λ_{ex} = 700 nm) for EuDO3A-AP^{ArOR} in PBS pH 7.4, data were fitted using $I = A \times P^n$ yielding $n = 2.01$; (C) 2P absorption spectrum (red) measured in PBS superimposed to the wavelength-doubled 1P absorption spectrum (black).

The 2P absorption properties of EuDO3A-AP^{ArOR} were determined by the two-photon excited fluorescence method. First, the quadratic dependence of the emitted Eu³⁺ intensity on laser power was checked under excitation at 700 nm with a Ti:sapphire laser (Fig. 3B). Then, the 2P absorption spectrum was measured. It matches nicely the wavelength-doubled 1P absorption spectrum (Fig. 3C). At 720 nm, the wavelength used in 2P microscopy experiments (vide infra), the 2P absorption cross-section, σ_{2P} , is 36 GM (1 GM = 10⁻⁵⁰ cm⁴·s·photon⁻¹), similar to the alkoxy-phenyl-ethynyl-picolinate antenna (35 GM)⁵¹ and ca. 10 times higher than that measured for an Eu³⁺ complex with a methoxy-phenyl-picolinamide antenna.⁴² At 720 nm, the 2P brightness, $B_{2P} = \sigma_{2P} \times \Phi_{Eu}$, of EuDO3A-AP^{ArOR} is 2.7 GM.

Relaxometric characterizations of GdDO3A-AP^{ArOR}

Since EuDO3A-AP^{ArOR} has a hydration number q of 1, its Gd³⁺ analogue appears to be a good candidate for MRI imaging. In

order to characterize the efficacy of GdDO3A-AP^{ArOR} and relate this to the microscopic parameters that govern the efficacy (relaxivity) of the complex, nuclear magnetic relaxation dispersion (NMRD) profiles, in combination with variable temperature ¹⁷O NMR experiments, were recorded. The NMRD profiles were recorded within the range of 0.01–600 MHz, at three different temperatures; 25, 37, and 50 °C (Fig. 4A). As temperature increased, the r_1 values decreased, indicating that the rotational correlation time is the limiting factor in the relaxivity, which is expected with a small molecular complex. The relaxivity at 20 MHz, 25 °C is 5.4 mM⁻¹ s⁻¹, consistent with a monohydrated complex of this size and which aligns well with the values found in the same conditions for GdHPDO3A (4.6 mM⁻¹ s⁻¹),⁵² and GdDO3A-AP (5.1 mM⁻¹ s⁻¹).⁴⁷

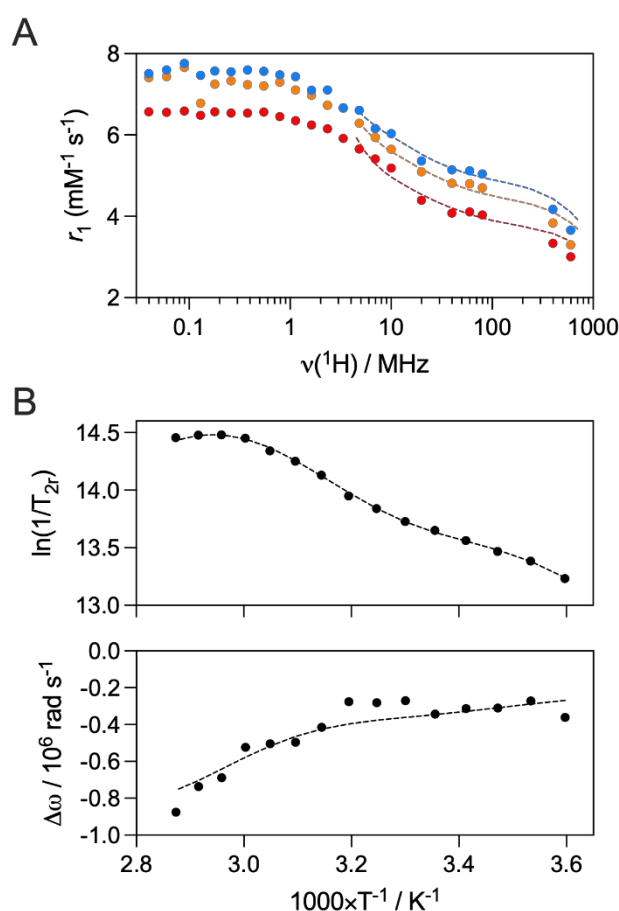


Fig. 4 (A) NMRD profile of GdDO3A-AP^{ArOR} (0.88 mM) at 25 °C (blue), 37 °C (orange), and 50 °C (red). (B) Temperature dependence of the ¹⁷O transverse relaxation rates (top) and ¹⁷O chemical shifts (bottom) of GdDO3A-AP^{ArOR} at 9.4 T (9 mM). The dotted lines represent the simultaneous fit of the experimental data points.

The reduced transverse relaxation rates ($1/T_{2r}$) were measured as a function of temperature to determine the water exchange rate, k_{ex} , while the reduced chemical shifts give access to the number of coordinated water molecules on the Gd³⁺ complex. The ¹⁷O-reduced transverse relaxation rates increase (up to ca. 333 K), followed by a plateau (Fig. 4B). The shape of the curve indicates that there are at least two isomers present in solution, most likely the SAP and TSAP coordination isomers



View Article Online

Table 1. The best-fit parameters obtained from the simultaneous fitting of the NMRD profiles at 298 K, 310 K, and 323 K, and the transverse ^{17}O relaxation rates and chemical shifts as a function of temperature at 9.4 T.

	Isomer	GdDO3A-AP ^{ArOR}	GdDO3A-AP ⁴⁷	GdHPDO3A ⁵²
r_1 ($\text{mM}^{-1} \text{s}^{-1}$) 20 MHz, 25 °C		5.4	5.1	4.6
k_{ex}^{298} (10^6s^{-1})	SAP	0.49 (3)	0.83	1.56
ΔH^\ddagger (kJ mol^{-1})	SAP	55 (3)	50	53
ΔS^\ddagger ($\text{kJ mol}^{-1} \text{K}^{-1}$)	SAP	+ 49	+ 36	+ 52
k_{ex}^{298} (10^6s^{-1})	TSAP	18 (3)	40	112
ΔH^\ddagger (kJ mol^{-1})	TSAP	42 (8)	27	15
τ_R^{298} (ps)		134 (3)	100	65

which display greatly different water exchange rates, as seen with GdHPDO3A,⁵² GdDOTA bisamide derivatives^{53,54} or GdDO3A-AP.⁴⁷ Thusly, a ^1H NMR study was performed (700 MHz at 288, 298, and 318 K) to determine the ratio between the SAP and TSAP isomers of EuDO3A-AP^{ArOR} in solution (Fig. S14). The SAP isomer is found to be the main isomer as already reported for the majority of DOTA-based complexes.⁵⁵ The ratio of SAP:TSAP is found to be 80:20, which is consistent with complexes reported in the literature with similar coordination sphere.^{46,47} Importantly, this ratio is constant over the range of temperature studied. The reduced chemical shifts measured are consistent with a monohydrated complex in solution, in accordance with the luminescence measurements on the Eu³⁺ complex.

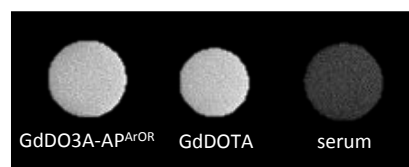
The NMRD profile, transverse ^{17}O relaxation rates, and ^{17}O chemical shifts were fitted simultaneously using Solomon-Bloembergen and Morgan (SBM) theory, while considering the relative populations of the two isomers in solution, to yield the microscopic parameters that govern the proton relaxivity of the complex (Table 1 and Table S1). The NMRD profiles were fitted in the range 4–600 MHz, where the effect of the electron spin relaxation, which is not well described by the SBM theory alone is negligible, and the SBM approach gives reliable information on dynamic processes like water exchange rate and rotational correlation time for small complexes.^{56,57}

Under the reasonable assumption that the rotational correlation time (τ_R) is the same for both SAP and TSAP species, a value of 134 ps is found. This value is larger than that of GdHPDO3A (65 ps) and GdDO3A-AP (100 ps), which is consistent with the larger size of GdDO3A-AP^{ArOR}. The fitting of the data yields $k_{\text{ex}} = 0.49 \times 10^6 \text{s}^{-1}$ for the SAP isomer and $k_{\text{ex}} = 18 \times 10^6 \text{s}^{-1}$ for the TSAP isomer. This is a well-known phenomenon, whereby the increased steric hindrance around the Gd³⁺-center of the TSAP isomer, results in a faster water exchange rate. It was previously observed that the introduction of a ketone pendant arm resulted in slow water exchange rates.^{47,58} In this case, the exchange rates of the SAP and TSAP isomers are even slower than those of GdDO3A-AP. This could be explained by the electronic effects of the benzene on the acetophenone, which decreases the electronic density on the ketone, therefore the steric crowding around Gd³⁺. In such complexes with positive activation entropy (dissociatively activated mechanism), this results in a lower water exchange rate.⁵⁹

Due to the presence of the hydrophobic biphenyl moiety, the complex could be prone to aggregation processes. Paramagnetic Relaxation Enhancements (PRE) measurements were performed at 60 MHz and 25 °C as a function of concentration (Fig. S15). A linear trend is observed, which demonstrates no aggregation of the complex in the concentration range studied (ca. 80 μM –8 mM).

The incorporation of a lipophilic group into a Gd³⁺-based contrast agent is a well-established method to promote non-covalent interactions between the CA and human serum albumin (HSA). This interaction has several advantages, such as increased relaxivity of the CA, mainly due to the increased rotational correlation time of the chelate, and a prolonged vascular retention time. Considering that biphenyl moieties have been leveraged multiple times to this effect, we considered that the biphenyl antenna present in DO3A-AP^{ArOR} could possibly interact with HSA in this manner. Thus, the relaxivity of GdDO3A-AP^{ArOR} in the presence of 0.6 mM HSA was measured at 60 MHz, 25 °C. An increase of ca. 110% in relaxivity was observed in the presence of HSA ($r_1 = 11.4 \text{mM}^{-1} \text{s}^{-1}$ vs. $r_1 = 5.38 \text{mM}^{-1} \text{s}^{-1}$ in HEPES buffer).

To further evaluate the potential of this complex as a contrast agent, T_1 -weighted phantom images were performed at 7 T, where the relaxivity of GdDO3A-AP^{ArOR} was measured in mouse blood serum and compared to GdDOTA, a Gd³⁺-based CA used clinically (Fig. 5). While GdDO3A-AP^{ArOR} did not retain its enhanced relaxivity at higher field strengths, it did display a similar signal intensity (3.89×10^4) to the clinically used GdDOTA (3.97×10^4) at 7 T, 25 °C (0.3 mM in mouse serum).

**Fig. 5** T_1 -weighted phantom images in mouse serum with GdDO3A-AP^{ArOR} and GdDOTA (0.3 mM) at room temperature. Images were acquired at 7 T using a spin echo sequence with TE = 10 ms, TR = 400 ms. The intensities are respectively 3.89×10^4 , 3.97×10^4 and 1.04×10^4 for GdDO3A-AP^{ArOR}, GdDOTA, and serum.

Stability

Given the *in vitro* potential of the system both in terms of luminescence and relaxivity, we wanted to assess its *in vivo* applicability. However, it is of prime importance to check the thermodynamic stability and kinetic inertness of the system



prior *in vivo* use. Macrocyclic lanthanides complexes based on DOTA or DOTA-monoamide systems are known to display high thermodynamic stability and kinetic inertness.⁶⁰ In this case, one ketone function is coordinating the Ln³⁺. Therefore, we first investigated the thermodynamic stability and kinetic inertness of EuDO3-AP^{ArOR} by competitions with DTPA at pH 7.4. EuDO3A-AP^{ArOR} was mixed with DTPA (1, 10 and 100 eq.) at pH 7.4 in PBS and the Eu³⁺ emission intensity was monitored after 24 h. At 1:1 and 1:10 EuDO3A-AP^{ArOR}/DTPA ratios, the Eu³⁺ emission intensity remained unchanged (Fig S16). A slight decrease of Eu³⁺ intensity was observed for a 1:100 ratio. This is indicative of a high thermodynamic stability or kinetic inertness. In more challenging conditions to assess the kinetic inertness and compare to other macrocyclic complexes, EuDO3-AP^{ArOR} was dissolved in HCl 1 M. The emission spectrum is the same as at pH 7.4 (Fig. S17A), indicating that the coordination sphere of the emissive Eu³⁺ species is not altered by the low pH. Under these conditions, the complex fully dissociates (Fig S17B). Given the very high proton concentration, the dissociation follows a pseudo-first order kinetics, and the dissociation rate is proportional to the total concentration of the complex [LnL]_t, with *k*_{obs} being the pseudo-first order rate constant:

$$-\frac{d[LnL]_t}{dt} = k_{obs}[LnL]_t$$

The dissociation half-life and *k*_{obs} values determined in 1 M HCl are presented in Table 2. The *k*_{obs} is one order of magnitude higher than that of GdDOTA,⁶¹ but two to three orders of magnitude lower than other macrocyclic compounds (GdDO3A⁶² or EuDO3Apic⁶³). Importantly, it is one order of magnitude lower than that of the commercially available GdHPDO3A.⁶⁴ The half-life in 1 M HCl is 5.3 h, which demonstrates the strong inertness of EuDO3-AP^{ArOR}.

Table 2. Rate constants characterizing the complexes dissociation determined in 1 M HCl at 298 K, and half-life in the same conditions

	<i>k</i> _{obs} (s ⁻¹)	<i>t</i> _{1/2} (min)
EuDO3A-AP ^{ArOR}	(3.6 ± 0.2) × 10 ⁻⁵	320 ± 20
GdDOTA ⁶¹	1.8 × 10 ⁻⁶	6418
GdDO3A ⁶²	2.3 × 10 ⁻²	0.5
EuDO3Apic ⁶³	2.0 × 10 ⁻³	5.7
GdHPDO3A ⁶⁴	2.6 × 10 ⁻⁴	44

In vivo MRI biodistribution in mice

Encouraged by the *in vitro* results, and the very high inertness of the complex, an *in vivo* MRI study was then carried out, where five healthy mice were injected with GdDO3A-AP^{ArOR} (100 μmol/kg). After intravenous administration of the contrast agent, an immediate increase in signal intensity was observed, with the signal enhancement peaking two minutes after injection for all organs (Fig. 6). The kidneys experienced the greatest signal enhancement over other organs. This indicates that the CA is cleared *via* the kidneys, with a negligible portion *via* the liver, which is expected for a small molecular complex. The clearance is fast as the signal enhancement in the main organs (liver, spleen and muscle) is negligible 50 min post-injection. *Ex vivo* biodistribution were also performed 1h post

injection and the Gd³⁺ content of various organs was measured *ex vivo* by Inductively Coupled Plasma Optical Emission Spectroscopy (ICP-OES) (Fig. 6). Less than 3 % of the injected dose per organ gram is found, showing a good elimination of the contrast agent after one hour. Interestingly, the Gd content one hour post injection is intermediate to that found for GdDOTA and Vasovist,⁶⁵ a blood-pool agent. This is consistent with the *in vitro* results showing some HSA binding, and a certainly longer circulation time than GdDOTA, but shorter than Vasovist. The excellent stability and inertness of GdDO3A-AP^{ArOR} and successful MRI experiments prompted us evaluate the potential of the Eu³⁺ analogue EuDO3A-AP^{ArOR} for *in vivo* 2P microscopy imaging in zebrafish embryos.

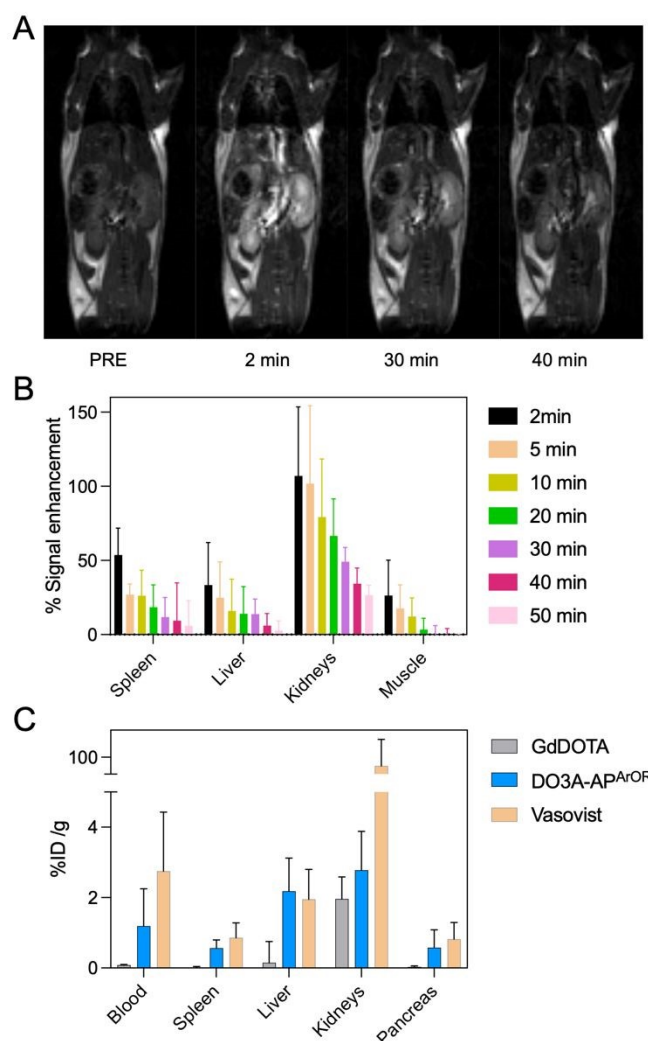


Fig. 6 (A) T₁-weighted MR images performed at 9.4 T of healthy mice pre-injection (left) and 2-, 30- and 40-minutes post *i.v.* injection of GdDO3A-AP^{ArOR} at 100 μmol/kg, (B) % of MRI signal enhancement in the spleen, liver, kidneys and muscle, 2-, 5-, 10-, 20-, 30-, 40- and 50-minutes post *i.v.* injection of GdDO3A-AP^{ArOR} at 100 μmol/kg (n = 5, ± SD). (C) Gd content in the blood, spleen, liver, kidneys, and pancreas measured by ICP-OES 1 h after injection of GdDO3A-AP^{ArOR} (blue), GdDOTA (grey), or Vasovist (orange). Data are presented in % of injected dose by organ mass (n = 5, ± SD).

In vivo 2P microscopy of zebrafish embryos



The use of zebrafish (*Danio rerio*) embryos is increasingly recognized as an alternative to testing on small mammals.^{66,67} Although imaging of zebrafish embryos with fluorescent probe is classical,⁶⁸ to our knowledge, examples of 2P zebrafish imaging with Ln³⁺ probes are scarce.^{7,69} First, the toxicity of EuDO3A-AP^{ArOR} in zebrafish embryos was studied at the single cell stage (see ESI for details). The development of embryos was observed at different time points (24, 48, 72, 96 and 120 h) post-injection. The viability was based on the morphology and the presence of heartbeat. Malformation including pericardial oedema, yolk sac oedema, spinal curvature and tail malformation was recorded. Dead embryos were removed immediately. The results shown in Fig. 7 demonstrate the mild toxicity of the EuDO3A-AP^{ArOR} *in vivo* (Fig. 7c). At 72 hpi (hours post-injection), an increase in the death rate of the EuDO3A-AP^{ArOR} injected group (25 %) compared to non-injected group (5 %) was observed. Further, an increase in the hatching rate in the PBS and EuDO3A-AP^{ArOR} injected groups (~70 %) compared to the non-injected group (25%) was recorded. EuDO3A-AP^{ArOR} did not induce higher morphological abnormalities than the non-injected or PBS injected group. The toxicity profile of EuDO3A-AP^{ArOR} remains constant from 72 hpi until 120 hpi.

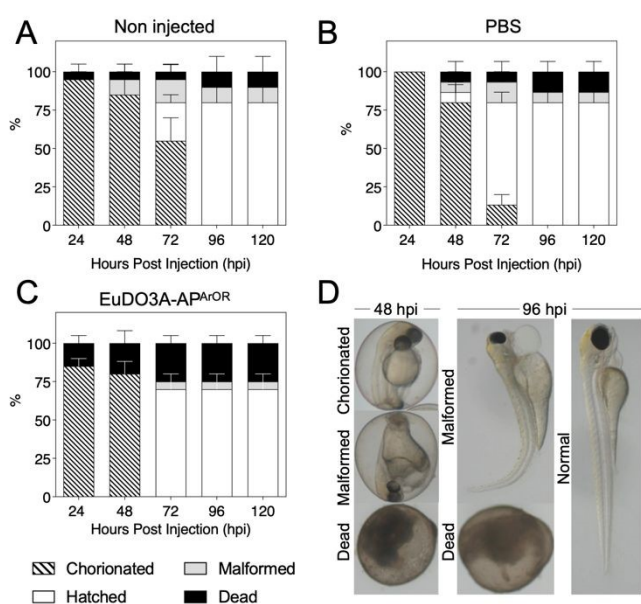


Fig. 7 Casper zebrafish embryo development expressed as percentages of chorionated, hatched, malformed and dead (a) without injection or after 1 nL of injection of (b) PBS or (c) EuDO3A-AP^{ArOR} (1 mM) at single cell stage. The observation was carried out after 24, 48, 72, 96 and 120 hpi. The total number of embryos is 20, 15 and 20 for non-injected, PBS and EuDO3A-AP^{ArOR} respectively. Data are presented as mean \pm SEM. (d) Representative images of the microscopic observation of embryos at 48 and 96 hpi using the microscope Zeiss Stemi 508.

Then, 2P microscopy imaging of zebrafish embryos was performed under 720 nm excitation with spectral detection 3 h after intravenous injection of EuDO3A-AP^{ArOR} (see ESI for details). As shown in Fig. 8A, the luminescence signal was collected with 570-640 bp filter and a long integration time of 131 μ s/pixel. The emission was detected in the heart, intersegmental vessels, caudal vein, caudal artery, primary head sinus and the inner optic circle. On the contrary, in the control

(no Eu³⁺ probe injected), the luminescence was detected mainly in the yolk, which usually shows high autofluorescence. In injected embryos, spectral detection (Fig. 8B) allowed for the discrimination of the broad autofluorescence signal with a maximum at ca. 460 nm and the Eu³⁺ emission with characteristic peaks at 580 nm and 620 nm. As expected, the latter was not detected in the control. Linear unmixing of the autofluorescence and Eu³⁺ signals is shown in Fig 8C. EuDO3A-AP^{ArOR} is clearly distributed in the cardiovascular circulatory system. Finally, the viability of embryos injected with EuDO3A-AP^{ArOR} was 80 % after 3 days post-injection, confirming its low toxicity. Therefore, EuDO3A-AP^{ArOR} is suitable to provide high-quality 2P images in zebrafish.

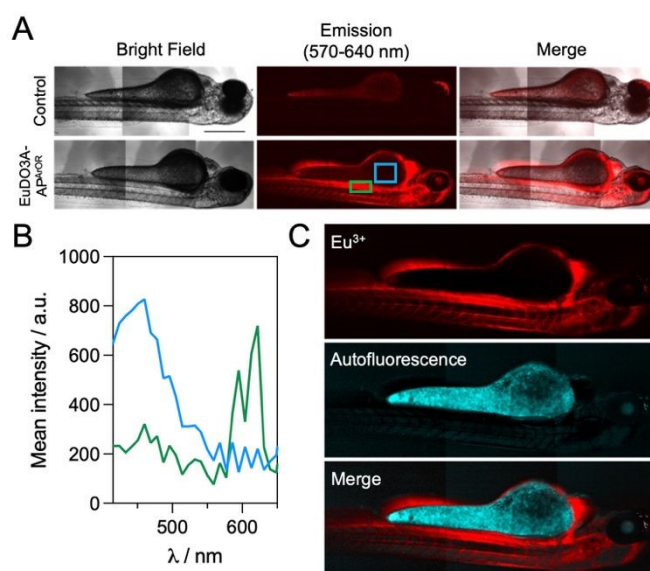


Fig. 8 (A) 2P microscopy imaging of 72 hours post-fertilization Casper zebrafish embryos intravenously injected with 10 nL of EuDO3A-AP^{ArOR} (1 mM) and observed 3 h after injection at 720 nm ($n = 5$ embryos). Scale bar 500 μ m. (B) Mean emission spectra in area outlined in blue and green in panel A. (C) Linear unmixing of autofluorescence and Eu³⁺ signal.

Preparation and characterization of the TAT conjugate

The *in vivo* applicability of the complex is well established both in MRI and luminescence to probe the extracellular environment. However, for bioimaging applications, it can be interesting to specifically vectorize the probe, for example, towards cancer cells or to make it cell-permeable in order to probe the intracellular environment and bring complementary information. This is generally achieved by coupling the probe to a peptide or a protein that brings recognition properties. Here, we choose to demonstrate the applicability of EuDO3A-AP^{ArOR} for 2P microscopy at the cell level by conjugating it to the well-known TAT cell penetrating peptide.^{41,42,70} The preparation of TAT conjugates with LnDO3Apic complexes, which have been described previously, relies on the coupling of a protected macrocyclic ligand to the peptide on resin, followed by (i) acidic cleavage from the resin and deprotection (side chains and ligand), (ii) HPLC purification and (iii) metalation with Ln³⁺. Here we opted for a more straightforward strategy, directly coupling the Ln³⁺ complex to the peptide on resin (Fig. 2B). The peptide



was elongated on Rink Amide resin using solid phase peptide synthesis following classical procedures for the Fmoc/tBu strategy. The N-terminal lysine was orthogonally protected with an alloc group. After selective removal of this group on resin using Pd⁰, EuDO3A-AP^{ArOR} was coupled to the peptide *via* its carboxylate handle using HATU/DIEA activation for 2 h. After resin cleavage and protecting group removal using TFA/H₂O/TIS, the conjugate was purified by HPLC and freeze-dried. The Eu³⁺ complex resisted the TFA treatment and the acidic HPLC conditions (H₂O/MeCN mixture with 0.1% TFA, pH *ca.* 2) and no Eu³⁺ release was observed, further validating the high inertness of the complex. Proper conjugation through the carboxylate handle on the electron donating group of the antenna was confirmed by mass spectrometry and Eu³⁺ luminescence properties.

The spectroscopic properties of mTAT[EuDO3A-AP^{ArOR}] are very similar to those of the parent Eu³⁺ complex (Fig. S13), with an identical absorption band, the same Eu³⁺ emission spectrum, which attests that the conjugation has not altered the Eu³⁺ coordination sphere, and identical Eu³⁺ luminescence lifetime (0.50 (2) ms) and quantum yield ($\Phi_{Eu} = 0.077$) within error margin. All this indicates that conjugation to the TAT peptide has no influence on the emission properties of EuDO3A-AP^{ArOR}.

In vitro 2P microscopy on living HeLa cells

In vitro imaging was attempted with live HeLa cells incubated with a mixture of mTAT[EuDO3A-AP^{ArOR}] and dFFLIPTAT, a dimeric cell penetrating peptide (sequence: (CFFLIIPRKRRQRRRG)₂, dimerized via a disulfide bound)) that helps TAT monomers such as mTAT[LnL] probes to enter live cells.^{71,41,42} Before conducting 2P microscopy on live HeLa cells, the cytotoxicity of the conjugate in co-incubation with dFFLIPTAT (1.5 μ M) was examined using the MTT assay (Fig. S18). After 48 h cell proliferation, no cytotoxicity was observed when the conjugate was incubated at 5 μ M and 10 μ M.

For microscopy experiments, HeLa cells were incubated with mTAT[EuDO3A-AP^{ArOR}] (5 μ M) and dFFLIPTAT (1.5 μ M) for 1 h before washing and imaging on a 2P microscope under 720 nm excitation using an APD (avalanche photodiode) for sensitive detection and a 580-680 nm bandpass filter to collect Eu³⁺ emission (Fig. 9A). The DIC (differential interference contrast) image shows HeLa cells with a phenotype of living cells in agreement with the MTT assay. The luminescence channel shows stained cells with diffuse red emission within the whole cell, typical of successful cytosolic delivery of the probe.^{40,42} The cell-to-cell intensity heterogeneity is a common feature of probes based on cell penetrating peptides.^{40,42,72,73} In order to confirm that the luminescence channel collects Eu³⁺ emission, a spectral image was recorded using the PMT array of the 2P microscope. Figure 9B shows the mean emission spectra of cells, recorded over the area outlined in red and blue in the DIC image. The ⁵D₀ → ⁷F_J, J = 1 and 2, emission bands of Eu³⁺ emission are unambiguously observed between 575 and 630 nm. The Eu³⁺ luminescence lifetime was measured in cells using the TSLIM method (Fig. 9C).⁷⁴ A value of 0.57 ± 0.03 ms (average over 15 measurements in three distinct cells) was found, similar to the one recorded in solution. This was surprising because with other

Eu³⁺ or Tb³⁺ probes featuring chelators that saturate the Ln³⁺ coordination sphere, we have always measured lifetimes *ca.* 30 % shorter in cells than in the cuvette.^{40,75} This shorter lifetime was proposed to be the consequence of additional de-excitation pathways in the cell via protein co-factors. In the present case, the higher lifetime suggests a change in the average hydration number of Eu³⁺, i.e. a partial replacement of the Eu³⁺-bound H₂O by a coordinating amino acid side chains of protein or small molecule. Note that in similar incubation conditions (1 h, 5 μ M probe), the non-conjugated complex EuDO3A-AP^{ArOR} is not detected within cells. Addition of DMSO (up to 5%) in the incubation medium to permeabilize membranes did not improve uptake. This demonstrates the value of conjugating the probe to a cell penetrating peptide. To sum up, despite its Eu³⁺-bound water molecule, EuDO3A-AP^{ArOR} conjugated to the TAT cell penetrating peptide allows 2P microscopy of live cells and gives high-quality images of live cells.

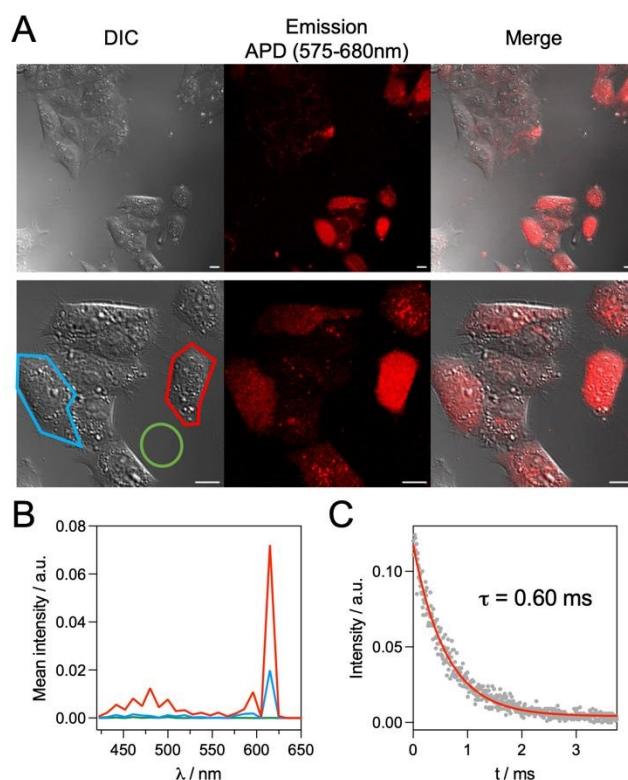


Fig. 9 2PM imaging ($\lambda_{ex} = 720$ nm) of living HeLa cells incubated 1 h with mTAT[EuDO3A-AP^{ArOR}] (5 μ M) and dFFLIPTAT (1.5 μ M) in RPMI medium. (A) *Left panel*: differential interference contrast (DIC) image; *Middle panel*: luminescence image recorded with 575-680 nm bp APD detection; *Right panel*: merge. Scale bars correspond to 10 μ m. (B) 2P-excited emission spectra (detected with a PMT array and averaged over the whole cell surface) of the cells outlined in red and blue and background (green). (C) Eu³⁺ luminescence decay in the cell outlined in red.

Conclusions

In this article, we have demonstrated that adding a π -conjugated extension to the acetophenone moiety of ligand DO3A-AP provides a luminescent Eu³⁺ complex, EuDO3A-AP^{ArOR},



with excellent 2P absorption properties compared to the picolinate analogue. Despite an Eu^{3+} -bound water molecule, which quenches Eu^{3+} emission and lowers luminescence properties, this complex has sufficiently good luminescence properties to make it suitable for *in vivo* 2P imaging of zebrafish and live cell 2P imaging. Compared to the picolinate analogue, the water molecule bound to Ln^{3+} proves to be an advantage, allowing MRI imaging *in vivo* with the Gd analogue, $\text{GdDO3A-AP}^{\text{ArOR}}$. This complex is therefore able to probe the extracellular environment *in vivo* both in MRI, with Gd^{3+} , and 2P microscopy imaging, with Eu^{3+} . Several DO3A- or DOTA-based ligand systems have already been described to elaborate by simple Ln^{3+} exchange both luminescent Eu^{3+} or MRI-active Gd^{3+} probes, with predictable MRI properties due to DO3A/DOTA scaffold.^{26–29} However, they were used in luminescence microscopy imaging with UV excitation. The system described here integrates a push-pull antenna that permits 2P excitation in the NIR, which is less damaging and allows better tissue penetration. The strong 2P absorption properties of this system provided for instances excellent quality microscopy images of zebrafish embryos. Finally, another advantage of this system is its pending carboxylate, which allows straightforward conjugation the $\text{LnDO3A-AP}^{\text{ArOR}}$ complexes to biomolecules such as peptides. This has been exemplified here with a TAT conjugate, a cell-penetrating peptide, allowing to obtain high-quality living cell microscopy images following 2P absorption despite the presence of the water molecule on the Ln^{3+} . Therefore, $\text{LnDO3A-AP}^{\text{ArOR}}$ complexes have a great potential and versatility for the safe development of efficient agents for MRI and 2P microscopy imaging.

Author contributions

Conceptualization: O. S., C. S. B., O. M., M. G.-B.; Investigation: B. C., L. M., L. M. A. A., D. A., G. M., S. M., S. E., V. M.-F., A. G., O. S.; Validation: O. S., C. S. B., M. G.-B., O. M., A. B., S. M. A. G., V. M.-F., D. B.; Writing (original draft): B. C., L. M., L. M. A. A., O. S., C. S. B., M. G.-B.; Writing (review & editing): all authors. Visualization: O. S., C. S. B., B. C., L. M., L. M. A. A.

Conflicts of interest

There are no conflicts to declare.

Data availability

The data supporting this article have been included as part of the Supplementary Information.

Acknowledgements

Agnès Pallier is acknowledged for performing ICP experiments. Authors thank the MO2VING platform for spectroscopic experiments. For zebrafish embryo imaging, authors acknowledge the imaging facility MRI, member of the France-BioImaging national infrastructure, supported by the French

National Research Agency (ANR-10-INBS-04, “Investments for the future”) and also, Nicolas Cubedo and Mireille Rosset from the aquatic model facility ZEFIX from MMDN/LPHI/CRBM/IGF. Cell 2P microscopy imaging experiments were done on Microcell core facility of the Institute for Advanced Biosciences (UGA – Inserm U1209 CNRS 5309). This facility belongs to the IBISA-ISdV platform, member of the national infrastructure France-BioImaging supported by the French National Research Agency (ANR-10-INBS-04). Authors acknowledge the Agence Nationale de la Recherche [LANTEN project (ANR-21-CE29-0018); and Zinc-Espionage project, (ANR-22-CE44-0041)], the Labex ARCANÉ and CBH-EUR-GS (ANR-17-EURE-0003) and the CEA FOCUS Biomarqueurs for financial support for financial support.

All animal experiments were carried out in accordance with the guidelines for animal experiments and under permission number 54201, from the French “Ministère de l’Enseignement Supérieur, de la Recherche et de l’Innovation”.

References

- J.-C. G. Bünzli and S. V. Eliseeva, in *Lanthanide Luminescence*, eds P. Hänninen and H. Härmä, Springer Berlin Heidelberg, 2011, pp. 1–45.
- J.-C. G. Bünzli, On the design of highly luminescent lanthanide complexes, *Coord. Chem. Rev.*, 2015, **293**, 19–47.
- C. Alexander, Z. Guo, P. B. Glover, S. Faulkner and Z. Pikramenou, Luminescent Lanthanides in Biorelated Applications: From Molecules to Nanoparticles and Diagnostic Probes to Therapeutics, *Chem. Rev.*, 2025, **125**, 2269–2370.
- M. Wang, Y. Kitagawa and Y. Hasegawa, Current Development of Lanthanide Complexes for Biomedical Applications, *Chem.-Asian J.*, 2024, **19**, e202400038.
- E. Mathieu, A. Sipos, E. Demeyere, D. Phipps, D. Sakaveli and K. E. Borbas, Lanthanide-based tools for the investigation of cellular environments, *Chem. Commun.*, 2018, **54**, 10021–10035.
- G.-Q. Jin, Y. Ning, J.-X. Geng, Z.-F. Jiang, Y. Wang and J.-L. Zhang, Joining the journey to near infrared (NIR) imaging: the emerging role of lanthanides in the designing of molecular probes, *Inorg. Chem. Front.*, 2020, **7**, 289–299.
- N. Hamon, A. Roux, M. Beyler, J.-C. Mulatier, C. Andraud, C. Nguyen, M. Maynadier, N. Bettache, A. Duperray, A. Grichine, S. Brasselet, M. Gary-Bobo, O. Maury and R. Tripiet, Pyclyen-Based Ln(III) Complexes as Highly Luminescent Bioprobes for In Vitro and In Vivo One- and Two-Photon Bioimaging Applications, *J. Am. Chem. Soc.*, 2020, **142**, 10184–10197.
- R. Sánchez-Fernández, I. Obregon-Gomez, A. Sarmiento, M. E. Vázquez and E. Pazos, Luminescent lanthanide metalloptides for biomolecule sensing and cellular imaging, *Chem. Commun.*, 2024, **60**, 12650–12661.
- D. Parker, J. D. Fradgley and K.-L. Wong, The design of responsive luminescent lanthanide probes and sensors, *Chem. Soc. Rev.*, 2021, **50**, 8193–8213.
- M. Sy, A. Nonat, N. Hildebrandt and L. J. Charbonnière, Lanthanide-based luminescence biolabelling, *Chem. Commun.*, 2016, **52**, 5080–5095.



- 11 J. M. Zwier, H. Bazin, L. Lamarque and G. Mathis, Luminescent Lanthanide Cryptates: from the Bench to the Bedside, *Inorg. Chem.*, 2014, **53**, 1854–1866.
- 12 M. C. Heffern, L. M. Matosziuk and T. J. Meade, Lanthanide Probes for Bioresponsive Imaging, *Chem. Rev.*, 2014, **114**, 4496–4539.
- 13 J. Wahsner, E. M. Gale, A. Rodríguez-Rodríguez and P. Caravan, Chemistry of MRI Contrast Agents: Current Challenges and New Frontiers, *Chem. Rev.*, 2019, **119**, 957–1057.
- 14 P. Caravan, D. Esteban-Gómez, A. Rodríguez-Rodríguez and C. Platas-Iglesias, Water exchange in lanthanide complexes for MRI applications. Lessons learned over the last 25 years, *Dalton Trans.*, 2019, **48**, 11161–11180.
- 15 P. Yue, T. Nagendraraj, G. Wang, Z. Jin and G. Angelovski, The role of responsive MRI probes in the past and the future of molecular imaging, *Chem. Sci.*, 2024, **15**, 20122–20154.
- 16 M. Liu, J. Gao, Y. Zhang, X. Zhou, Y. Wang, L. Wu, Z. Tian and J.-H. Tang, Recent advances in bioresponsive macrocyclic gadolinium(III) complexes for MR imaging and therapy, *Dalton Trans.*, 2025, **54**, 6741–6777.
- 17 M. V. C. Jordan, S.-T. Lo, S. Chen, C. Preihs, S. Chirayil, S. Zhang, P. Kapur, W.-H. Li, L. M. D. De Leon-Rodríguez, A. J. M. Lubag, N. M. Rofsky and A. D. Sherry, Zinc-sensitive MRI contrast agent detects differential release of Zn(II) ions from the healthy vs. malignant mouse prostate, *Proc. Natl. Acad. Sci. U. S. A.*, 2016, **113**, E5464–E5471.
- 18 M. Isaac, A. Pallier, F. Szeremeta, P.-A. Bayle, L. Barantin, C. S. Bonnet and O. Sènèque, MRI and luminescence detection of Zn²⁺ with a lanthanide complex–zinc finger peptide conjugate, *Chem. Commun.*, 2018, **54**, 7350–7353.
- 19 M. Sanadar, K. Zimmerer, H. Martin, A. Pallier, B. Vileño, P. Faller, A. Sour and C. S. Bonnet, Exploring Bioinspired Ln³⁺ Complexes for Cu²⁺ Detection: Design and Efficacy as MRI Contrast Agents, *Eur. J. Inorg. Chem.*, 2025, **28**, e202500049.
- 20 C. Moreau, T. Lukačević, A. Pallier, J. Sobilo, S. Aci-Sèche, N. Garnier, S. Mème, É. Tóth and S. Lacerda, Peptide-Conjugated MRI Probe Targeted to Netrin-1, a Novel Metastatic Breast Cancer Biomarker, *Bioconjugate Chem.*, 2024, **35**, 265–275.
- 21 F. Oukhatar, S. Mème, W. Mème, F. Szeremeta, N. K. Logothetis, G. Angelovski and É. Tóth, MRI Sensing of Neurotransmitters with a Crown Ether Appended Gd³⁺ Complex, *ACS Chem. Neurosci.*, 2015, **6**, 219–225.
- 22 C. S. Bonnet and É. Tóth, Towards highly efficient, intelligent and bimodal imaging probes: Novel approaches provided by lanthanide coordination chemistry, *Comptes Rendus Chimie*, 2010, **13**, 700–714.
- 23 C. S. Bonnet, F. Buron, F. Caille, C. M. Shade, B. Drahos, L. Pellegatti, J. Zhang, S. Villette, L. Helm, C. Pichon, F. Suzenet, S. Petoud and E. Toth, Pyridine-Based Lanthanide Complexes Combining MRI and NIR Luminescence Activities, *Chem.-Eur. J.*, 2012, **18**, 1419–1431.
- 24 B. Song, J. Jiang, H. Yan, S. Huang and J. Yuan, A tumor-targetable probe based on europium(III)/gadolinium(III) complex-conjugated transferrin for dual-modal time-gated luminescence and magnetic resonance imaging of cancerous cells in vitro and in vivo, *J. Mater. Chem. B*, 2023, **11**, 4346–4353.
- 25 S. Laurent, L. Vander Elst, C. Galaup, N. Leygue, S. Boutry, C. Picard and Robert. N. Muller, Bifunctional Gd(III) and Tb(III) chelates based on a pyridine-bis(iminodiacetate) platform, suitable optical probes and contrast agents for magnetic resonance imaging, *Contrast Media Mol. Imaging*, 2014, **9**, 300–312. DOI: 10.1039/D5SC06902E
- 26 J. He, C. S. Bonnet, S. V. Eliseeva, S. Lacerda, T. Chauvin, P. Retailleau, F. Szeremeta, B. Badet, S. Petoud, É. Tóth and P. Durand, Prototypes of Lanthanide(III) Agents Responsive to Enzymatic Activities in Three Complementary Imaging Modalities: Visible/Near-Infrared Luminescence, PARACEST-, and T1-MRI, *J. Am. Chem. Soc.*, 2016, **138**, 2913–2916.
- 27 Y. Zhang, X. Ma, H.-F. Chau, W. Thor, L. Jiang, S. Zha, W.-Y. Fok, H.-N. Mak, J. Zhang, J. Cai, C.-F. Ng, H. Li, D. Parker, L. Li, G.-L. Law and K.-L. Wong, Lanthanide–Cyclen–Camptothecin Nanocomposites for Cancer Theranostics Guided by Near-Infrared and Magnetic Resonance Imaging, *ACS Appl. Nano Mater.*, 2021, **4**, 271–278.
- 28 T.-L. Cheung, L. K. B. Tam, W.-S. Tam, L. Zhang, H.-Y. Kai, W. Thor, Y. Wu, P.-L. Lam, Y.-H. Yeung, C. Xie, H.-F. Chau, W.-S. Lo, T. Zhang and K.-L. Wong, Facile Peptide Macrocyclization and Multifunctionalization via Cyclen Installation, *Small Methods*, 2024, e2400006.
- 29 R. Jouclas, S. Laine, S. V. Eliseeva, J. Mandel, F. Szeremeta, P. Retailleau, J. He, J.-F. Gallard, A. Pallier, C. S. Bonnet, S. Petoud, P. Durand and É. Tóth, Lanthanide-Based Probes for Imaging Detection of Enzyme Activities by NIR Luminescence, T1- and ParaCEST MRI, *Angew. Chem., Int. Ed.*, 2024, **63**, e202317728.
- 30 C. A. Foster, D. Sneddon, L. Hacker, E. T. Sarson, M. Robertson, D. Sokolova, L. A. W. Martin, M. F. Allen, A. Khrapichev, K. A. Vincent, E. M. Hammond, S. J. Conway and S. Faulkner, LnDOTA Releasing Probes for Luminescence and Magnetic Resonance Imaging, *Inorg. Chem.*, 2025, **64**, 6640–6647.
- 31 B. Woolley, Y. Wu, L. Xiong, H.-F. Chau, J. Zhang, G.-L. Law, K.-L. Wong and N. J. Long, Lanthanide–tetrazine probes for bio-imaging and click chemistry, *Chem. Sci.*, 2025, **16**, 3588–3597.
- 32 S. I. Weissman, Intramolecular Energy Transfer: The Fluorescence of Complexes of Europium, *J. Chem. Phys.*, 1942, **10**, 214–217.
- 33 M. Pawlicki, H. A. Collins, R. G. Denning and H. L. Anderson, Two-Photon Absorption and the Design of Two-Photon Dyes, *Angew. Chem., Int. Ed.*, 2009, **48**, 3244–3266.
- 34 G. Piszczek, B. P. Maliwal, I. Gryczynski, J. Dattelbaum and J. R. Lakowicz, Multiphoton ligand-enhanced excitation of lanthanides, *J. Fluoresc.*, 2001, **11**, 101–107.
- 35 M. H. V. Werts, N. Nerambourg, D. Pélégry, Y. L. Grand and M. Blanchard-Desce, Action cross sections of two-photon excited luminescence of some Eu(III) and Tb(III) complexes, *Photochem. Photobiol. Sci.*, 2005, **4**, 531–538.
- 36 A. Picot, A. D'Aleo, P. L. Baldeck, A. Grichine, A. Duperray, C. Andraud and O. Maury, Long-lived two-photon excited luminescence of water-soluble europium complex: Applications in biological imaging using two-photon scanning microscopy, *J. Am. Chem. Soc.*, 2008, **130**, 1532–1533.
- 37 A. D'Aléo, A. Bourdolle, S. Brustlein, T. Fauquier, A. Grichine, A. Duperray, P. L. Baldeck, C. Andraud, S. Brasselet and O. Maury, Ytterbium-Based Bioprobes for Near-Infrared Two-Photon Scanning Laser Microscopy Imaging, *Angew. Chem., Int. Ed.*, 2012, **51**, 6622–6625.
- 38 R. Lengacher, K. E. Martin, D. Śmiłowicz, H. Esseln, P. Lotlikar, A. Grichine, O. Maury and E. Boros, Targeted, Molecular Europium(III) Probes Enable Luminescence-Guided Surgery and 1 Photon Post-Surgical Luminescence Microscopy of Solid Tumors, *J. Am. Chem. Soc.*, 2023, **145**, 24358–24366.
- 39 J.-H. Choi, G. Fremy, T. Charnay, N. Fayad, J. Pécaut, S. Erbek, N. Hildebrandt, V. Martel-Frchet, A. Grichine and O. Sènèque,



- Luminescent Peptide/Lanthanide(III) Complex Conjugates with Push–Pull Antennas: Application to One- and Two-Photon Microscopy Imaging, *Inorg. Chem.*, 2022, **61**, 20674–20689.
- 40 K. P. Malikidogo, T. Charnay, D. Ndiaye, J.-H. Choi, L. Bridou, B. Chartier, S. Erbek, G. Micouin, A. Banyasz, O. Maury, V. Martel-Frchet, A. Grichine and O. S  n  que, Efficient cytosolic delivery of luminescent lanthanide bioprobes in live cells for two-photon microscopy, *Chem. Sci.*, 2024, **15**, 9694–9702.
 - 41 J.-H. Choi, A. Nhari, T. Charnay, B. Chartier, L. Bridou, G. Micouin, O. Maury, A. Banyasz, S. Erbek, A. Grichine, V. Martel-Frchet, F. Thomas, J. K. Molloy and O. S  n  que, Carbazole-Based Eu³⁺ Complexes for Two-Photon Microscopy Imaging of Live Cells, *Inorg. Chem.*, 2025, **64**, 2006–2019.
 - 42 B. Chartier, A. Grichine, L. Bridou, A. Nhari, G. Micouin, A. Banyasz, D. Boturyn, J. K. Molloy, S. Erbek, V. Martel-Frchet, O. Maury and O. S  n  que, Amido/alkoxy–aryl–aryl–picolinate push–pull antennas for two-photon sensitization of Eu³⁺ luminescence, *Inorg. Chem. Front.*, 2025, **12**, 3313–3323.
 - 43 L. Bridou, L. Collobert, K. P. Malikidogo, S. R. Kiraev, M. Hojorot, N. Hamon, A. T. Bui, F. Riob  , A. Banyasz, M. Beyler, R. Tripier, O. S  n  que and O. Maury, Exploring Photophysical Properties and Sensitivity to Oxygen in Anisoyl-Picolinate Antenna Conjugated to Azamacrocycles, *Inorg. Chem.*, 2025, **64**, 13635–13646.
 - 44 A. Beeby, L. M. Bushby, D. Maffeo and J. a. G. Williams, Intramolecular sensitisation of lanthanide(III) luminescence by acetophenone-containing ligands: the critical effect of para-substituents and solvent, *J. Chem. Soc.-Dalton Trans.*, 2002, 48–54.
 - 45 M. Tropiano, A. M. Kenwright and S. Faulkner, Lanthanide Complexes of Azidophenacyl-DO3A as New Synthons for Click Chemistry and the Synthesis of Heterometallic Lanthanide Arrays, *Chem.-Eur. J.*, 2015, **21**, 5697–5699.
 - 46 J. D. Routledge, M. W. Jones, S. Faulkner and M. Tropiano, Kinetically Stable Lanthanide Complexes Displaying Exceptionally High Quantum Yields upon Long-Wavelength Excitation: Synthesis, Photophysical Properties, and Solution Speciation, *Inorg. Chem.*, 2015, **54**, 3337–3345.
 - 47 L. Leone, D. Esteban-G  mez, C. Platas-Iglesias, M. Milanesio and L. Tei, Accelerating water exchange in Gd(III)–DO3A-derivatives by favouring the dissociative mechanism through hydrogen bonding, *Chem. Commun.*, 2019, **55**, 513–516.
 - 48 L. Leone, S. Camorali, A. Freire-Garc  a, C. Platas-Iglesias, D. E. Gomez and L. Tei, Scrutinising the role of intramolecular hydrogen bonding in water exchange dynamics of Gd(III) complexes, *Dalton Trans.*, 2021, **50**, 5506–5518.
 - 49 B. Jagdish, G. L. Brickert-Albrecht, G. S. Nichol, E. A. Mash and N. Raghunand, On the synthesis of 1,4,7-tris(tert-butoxycarbonylmethyl)-1,4,7,10-tetraazacyclododecane, *Tetrahedron Lett.*, 2011, **52**, 2058–2061.
 - 50 A. Beeby, I. M. Clarkson, R. S. Dickins, S. Faulkner, D. Parker, L. Royle, A. S. de Sousa, J. A. G. Williams and M. Woods, Non-radiative deactivation of the excited states of europium, terbium and ytterbium complexes by proximate energy-matched OH, NH and CH oscillators: an improved luminescence method for establishing solution hydration states, *J. Chem. Soc., Perkin Trans. 2*, 1999, 493–504.
 - 51 S. Mizzoni, S. Ruggieri, A. Sickinger, F. Riob  , L. Guy, M. Roux, G. Micouin, A. Banyasz, O. Maury, B. Baguenard, A. Bensalah-Ledoux, S. Guy, A. Grichine, X.-N. Nguyen, A. Cimarelli, M. Sanadar, A. Melchior and F. Piccinelli, Circularly polarized activity from two photon excitable europium and samarium chiral bioprobes, *J. Mater. Chem. C*, 2023, **11**, 4188–4202.
 - 52 D. Delli Castelli, M. C. Caligara, M. Botta, E. Terreno and S. Aime, Combined High Resolution NMR and 1H and 17O Relaxometric Study Sheds Light on the Solution Structure and Dynamics of the Lanthanide(III) Complexes of HPDO3A, *Inorg. Chem.*, 2013, **52**, 7130–7138.
 - 53 S. Zhang, Z. Kovacs, S. Burgess, S. Aime, E. Terreno and A. D. Sherry, DOTA-bis(amide)lanthanide Complexes: NMR Evidence for Differences in Water-Molecule Exchange Rates for Coordination Isomers, *Chem.-Eur. J.*, 2001, **7**, 288–296.
 - 54 A. Pagoto, R. Stefania, F. Garelli, F. Arena, G. Digilio, S. Aime and E. Terreno, Paramagnetic Phospholipid-Based Micelles Targeting VCAM-1 Receptors for MRI Visualization of Inflammation, *Bioconjugate Chem.*, 2016, **27**, 1921–1930.
 - 55 S. Aime, M. Botta, Z. Garda, B. E. Kucera, G. Tircso, V. G. Young and M. Woods, Properties, Solution State Behavior, and Crystal Structures of Chelates of DOTMA, *Inorg. Chem.*, 2011, **50**, 7955–7965.
 - 56 P. H. Fries and E. Belorizky, Electronic relaxation of paramagnetic metal ions and NMR relaxivity in solution: Critical analysis of various approaches and application to a Gd(III)-based contrast agent, *J. Chem. Phys.*, 2005, **123**, 124510.
 - 57 P. Mi  ville, H. Jaccard, F. Reviriego, R. Tripier and L. Helm, Synthesis, complexation and NMR relaxation properties of Gd³⁺ complexes of Mes(DO3A)₃, *Dalton Trans.*, 2011, **40**, 4260–4267.
 - 58 K. N. Green, S. Viswanathan, F. A. Rojas-Quijano, Z. Kovacs and A. D. Sherry, Europium(III) DOTA-Derivatives Having Ketone Donor Pendant Arms Display Dramatically Slower Water Exchange, *Inorg. Chem.*, 2011, **50**, 1648–1655.
 - 59   . T  th, L. Helm and A. Merbach, in *The Chemistry of Contrast Agents in Medical Magnetic Resonance Imaging*, eds A. Merbach, L. Helm and   . T  th, John Wiley & Sons, Ltd, 2013, pp. 25–81.
 - 60 E. Br  cher, G. Tircs  , Z. Baranyai, Z. Kov  cs and A. D. Sherry, in *The Chemistry of Contrast Agents in Medical Magnetic Resonance Imaging*, John Wiley and Sons, 2013, pp. 157–208.
 - 61 Z. Baranyai, Z. P  link  s, F. Uggeri, A. Maiocchi, S. Aime and E. Br  cher, Dissociation Kinetics of Open-Chain and Macrocyclic Gadolinium(III)-Aminopolycarboxylate Complexes Related to Magnetic Resonance Imaging: Catalytic Effect of Endogenous Ligands, *Chem.-Eur. J.*, 2012, **18**, 16426–16435.
 - 62 A. Tak  cs, R. Napolitano, M. Purgel, A. C. B  nyei, L. Z  k  ny, E. Br  cher, I. T  th, Z. Baranyai and S. Aime, Solution Structures, Stabilities, Kinetics, and Dynamics of DO3A and DO3A–Sulphonamide Complexes, *Inorg. Chem.*, 2014, **53**, 2858–2872.
 - 63 M. Regueiro-Figueroa, B. Bensenane, E. Ruscak, D. Esteban-Gomez, L. J. Charbonni  re, G. Tircso, I. Toth, A. de Blas, T. Rodr  guez-Blas and C. Platas-Iglesias, Lanthanide dota-like Complexes Containing a Picolinate Pendant: Structural Entry for the Design of Ln(III)-Based Luminescent Probes, *Inorg. Chem.*, 2011, **50**, 4125–4141.
 - 64   . T  th, R. Kir  ly, J. Platzek, B. Rad  chel and E. Br  cher, Equilibrium and kinetic studies on complexes of 10-[2,3-dihydroxy-(1-hydroxymethyl)-propyl]-1,4,7,10-tetraazacyclododecane-1,4,7-triacetate, *Inorganica Chim. Acta*, 1996, **249**, 191–199.
 - 65 R. B. Lauffer, D. J. Parmelee, S. U. Dunham, H. S. Ouellet, R. P. Dolan, S. Witte, T. J. McMurphy and R. C. Walovitch, MS-325: albumin-targeted contrast agent for MR angiography., *Radiology*, 1998, **207**, 529–538.



ARTICLE

Journal Name

- 66 B. Bauer, A. Mally and D. Liedtke, Zebrafish Embryos and Larvae as Alternative Animal Models for Toxicity Testing, *Int.J. Mol. Sci.*, 2021, **22**, 13417.
- 67 T.-Y. Choi, T.-I. Choi, Y.-R. Lee, S.-K. Choe and C.-H. Kim, Zebrafish as an animal model for biomedical research, *Exp. Mol. Med.*, 2021, **53**, 310–317.
- 68 S.-K. Ko, X. Chen, J. Yoon and I. Shin, Zebrafish as a good vertebrate model for molecular imaging using fluorescent probes, *Chem. Soc. Rev.*, 2011, **40**, 2120–2130.
- 69 J. Zheng, Q. Zhan, L. Jiang, D. Xing, T. Zhang and K.-L. Wong, A bioorthogonal time-resolved luminogenic probe for metabolic labelling and imaging of glycans, *Inorg. Chem. Front.*, 2020, **7**, 4062–4069.
- 70 E. Vivès, P. Brodin and B. Lebleu, A truncated HIV-1 Tat protein basic domain rapidly translocates through the plasma membrane and accumulates in the cell nucleus, *J. Biol. Chem.*, 1997, **272**, 16010–16017.
- 71 J. Allen and J.-P. Pellois, Hydrophobicity is a key determinant in the activity of arginine-rich cell penetrating peptides, *Sci. Rep.*, 2022, **12**, 15981.
- 72 A. Erazo-Oliveras, K. Najjar, L. Dayani, T.-Y. Wang, G. A. Johnson and J.-P. Pellois, Protein delivery into live cells by incubation with an endosomolytic agent, *Nat. Methods*, 2014, **11**, 861–867.
- 73 M. Serulla, P. Anees, A. Hallaj, E. Trofimenko, T. Kalia, Y. Krishnan and C. Widmann, Plasma membrane depolarization reveals endosomal escape incapacity of cell-penetrating peptides, *Eur. J. Pharm. Biopharm.*, 2023, **184**, 116–124.
- 74 A. Grichine, A. Haefele, S. Pascal, A. Duperray, R. Michel, C. Andraud and O. Maury, Millisecond lifetime imaging with a europium complex using a commercial confocal microscope under one or two-photon excitation, *Chem. Sci.*, 2014, **5**, 3475–3485.
- 75 B. Chartier, N. Hamon, D. Akl, A. Sickinger, L. Corne, G. Micouin, A. Banyasz, O. Maury, S. Erbek, V. Martel-Frchet, A. Grichine, M. Beyler, O. Sénèque and R. Tripiet, Clickable Pyclyen-Based Luminescent Lanthanide Complexes: Application to Two-Photon Microscopy, *Chem.-Eur. J.*, 2025, **31**, e02044.

View Article Online
DOI: 10.1039/D5SC06902E



The data supporting this article have been included as part of the Supplementary Information.

